Journal of Systems Engineering and Electronics
Vol. 35, No. 1, February 2024, pp.43 – 54

Adaptive detection of range-spread targets in homogeneous and partially homogeneous clutter plus subspace interference

JIAN Tao[1,*], HE Jia[1], WANG Bencai[2], LIU Yu[1], XU Congan[1], and XIE Zikeng[1]

1. Research Institute of Information Fusion, Naval Aviation University, Yantai 264001, China;
2. Air Force Early Warning Academy, Wuhan 430019, China

Abstract: Adaptive detection of range-spread targets is considered in the presence of subspace interference plus Gaussian clutter with unknown covariance matrix. The target signal and interference are supposed to lie in two linearly independent subspaces with deterministic but unknown coordinates. Relying on the two-step criteria, two adaptive detectors based on Gradient tests are proposed, in homogeneous and partially homogeneous clutter plus subspace interference, respectively. Both of the proposed detectors exhibit theoretically constant false alarm rate property against unknown clutter covariance matrix as well as the power level. Numerical results show that, the proposed detectors have better performance than their existing counterparts, especially for mismatches in the signal steering vectors.

Keywords: adaptive detection, subspace interference, constant false alarm rate, Gradient test, partially homogeneous environment.

DOI: 10.23919/JSEE.2023.000147

1. Introduction

Adaptive detection of wideband radar target has garnered increasing attention in radar signal processing field for recent decades [1−3]. The range-spread target resulted from the spread of wideband radar target energy into the adjacent range cells are therefore more concerned [4−6]. Moreover, many adaptive detectors have been proposed for multichannel adaptive target detection in Gaussian clutter with unknown covariance matrix in the open literature [7,8], such as the generalized likelihood ratio test (GLRT), Rao test, and Wald test. Liu et al. mainly discussed the case of homogeneous environment (HE) [7], while De Maio et al. discussed the case of partially HE (PHE) [8]. Note that the test data have the identical clutter covariance matrix with the training data in HE [9−11], but the clutter covariance matrix of test data coincides with that of training data only up to a scaling factor in PHE [12−14].

It is noteworthy that none of the aforementioned works have taken the interference into account. However, due to the existence of natural or man-made interference sources, such as electronic countermeasures or civil broadcasting systems, it may be necessary to consider interference in the design procedure of detector. The interference is usually assumed to lie in a subspace to describe the uncertainties of interference pointing and/or Doppler frequency in many realistic scenarios [15−19]. In the presence of subspace interference and Gaussian clutter, the detectors are derived for range-spread targets in both HE and PHE, based on GLRT in [20] and Rao test in [21], respectively. More precisely, for HE, the one-step detectors are denoted as 1S-GLRT-HE and 1S-Rao-HE, while the two-step detectors are denoted as 2S-GLRT-HE and 2S-Rao-HE [20,21]. Similarly, the detectors for PHE are named as 1S-GLRT-PHE, 1S-Rao-PHE, 2S-GLRT-PHE, and 2S-Rao-PHE [20,21]. In [22], the Wald test has been designed, but for point-like target detection. In addition, according to the Gradient test criterion, two adaptive detectors (Gradient-HE and Gradient-PHE) are devised in HE and PHE, respectively, without considering interference [23].

In many practical scenarios, mismatches in signal steering vectors often occur, due to wavefront distortions, array calibration errors, etc. [24]. For example, in radar search mode, the detectors are expected to be robust to the mismatches in signal steering vectors [25,26]. For rank-one signals, the target steering vector is a fixed and fully known, which is unable to cope with the above mismatches. A feasible means to tolerate the mismatches is

Manuscript received May 16, 2022.
*Corresponding author.
This work was supported by the National Natural Science Foundation of China (61971432), Taishan Scholar Project of Shandong Province (tsqn201909156), and the Outstanding Youth Innovation Team Program of University in Shandong Province (2019KJN031).

using a subspace model [6−8], where the target signal lies in a multi-rank subspace and its coordinate is unknown.

As the parameters including clutter covariance matrix, subspace coordinates of target signal and interference are unknown, there is no uniformly most powerful detector for the problem of detecting range-spread targets in subspace interference plus Gaussian clutter [27−29]. It is reasonable to investigate new test techniques different from the GLRT, Rao, and Wald tests. In this work, relying on the two-step criteria, two adaptive detectors based on Gradient tests (named as 2S-Gradient-HE and 2S-Gradient-PHE) are proposed for range-spread targets modeled as subspace signals, in HE and PHE plus subspace interference, respectively. Both of the proposed detectors are proved to possess the constant false alarm rate (CFAR) properties under the design assumptions. In addition, the numerical results show that, compared with the existing competitors, the proposed two-step Gradient tests have better performance, especially when the mismatch occurs in the signal steering vectors.

The rest of this paper is organized as follows. Section 2 presents the target detection problem to be solved. Section 3 derives the Gradient tests for range-spread targets in HE and PHE. Section 4 provides CFAR property analyses for the proposed detectors theoretically. The performance assessment and comparison are provided in Section 5. Finally, Section 6 concludes the paper.

2. Problem formulation

Assume that a radar system collects data from N channels (spatial and/or temporal). The data returns from the cells under test are properly sampled and organized to form N-dimensional vectors. Moreover, assume that the data recorded from adjacent K range cells under test can be organized as $\boldsymbol{Z} \in \mathbf{C}^{N\times K}$, where $\mathbf{C}^{m\times n}$ denote an $m\times n$ complex-value space. And the range migration is neglected. In addition, a set of target-free training data denoted by collected from R range cells is assumed to be available to estimate unknown clutter covariance matrix. We need to decide between the null hypotheses H_0 and the valid hypotheses H_1, where the hypothesis H_1 or H_0 supposes that a range-spread target is present or absent in the received data. Hence, the detection problem at hand can be formulated as the following binary hypothesis test:

$$\mathrm{H}_0: \begin{cases} \boldsymbol{z}_t \sim \mathrm{CN}(\boldsymbol{J}\boldsymbol{q}_t, \gamma\boldsymbol{M}), & t=1,2,\cdots,K \\ \boldsymbol{y}_t \sim \mathrm{CN}(\boldsymbol{0}, \boldsymbol{M}), & t=1,2,\cdots,R \end{cases}, \tag{1}$$

$$\mathrm{H}_1: \begin{cases} \boldsymbol{z}_t \sim \mathrm{CN}(\boldsymbol{H}\boldsymbol{p}_t + \boldsymbol{J}\boldsymbol{q}_t, \gamma\boldsymbol{M}), & t=1,2,\cdots,K \\ \boldsymbol{y}_t \sim \mathrm{CN}(\boldsymbol{0}, \boldsymbol{M}), & t=1,2,\cdots,R \end{cases}. \tag{2}$$

(i) The symbol "$\sim$" means "is distributed as"; $\mathrm{CN}(\boldsymbol{r}, \boldsymbol{M})$ implies a circularly symmetric, complex Gaussian distribution with mean vector $\boldsymbol{r}$ and covariance matrix $\boldsymbol{M}$.

(ii) $\boldsymbol{z}_t \in \mathbf{C}^{N\times 1}$ is the tth column of test data $\boldsymbol{Z}$, which denotes the returns from the tth range cell under test.

(iii) $\boldsymbol{y}_t \in \mathbf{C}^{N\times 1}$ is the tth column of training data $\boldsymbol{Y}$, which denotes the returns from the tth training range cell.

(iv) $\boldsymbol{H} \in \mathbf{C}^{N\times p}$ and $\boldsymbol{J} \in \mathbf{C}^{N\times q}$ denote the known full-column-rank unitary matrixes for target signals and interference signals, respectively. $\boldsymbol{H}$ and $\boldsymbol{J}$ are supposed to be linearly independent, and let $\boldsymbol{B} = [\boldsymbol{H}\ \boldsymbol{J}]$ be a full-column-rank augmented matrix such that $p+q \leqslant N$.

(v) $\boldsymbol{p}_t \in \mathbf{C}^{p\times 1}$ and $\boldsymbol{q}_t \in \mathbf{C}^{q\times 1}$ imply determinate but unknown complex coordinate vectors for target signals and interference signals in the tth range cell under test, respectively.

(vi) $\boldsymbol{M}$ denotes the unknown Hermitian positive definite covariance matrix of training data, and $\gamma > 0$ is a scaling factor accounting for unknown power mismatch between the test data and training data. Note that $\gamma = 1$ in HE while $\gamma \neq 1$ in PHE.

3. Detector design

In this section, the two-step criterion is adopted to design Gradient tests for the detection problem in (1) and (2). First, it is assumed that the clutter covariance matrix $\boldsymbol{M}$ is known, and derive a Gradient test statistic by utilizing test data. Next, we obtain the maximum likelihood (ML) estimate of $\boldsymbol{M}$ by only using the training data, which is then employed to replace the true clutter covariance matrix in the detection statistic derived before. The specific implementation steps are as follows.

In the first step, it is easy to obtain the probability density function (PDF) of $\boldsymbol{Z} = [\boldsymbol{z}_1, \boldsymbol{z}_2, \cdots, \boldsymbol{z}_K]$ under hypothesis H_0 [30] as follows:

$$f_0(\boldsymbol{Z}) = \frac{\exp\left\{-\mathrm{tr}\left[\boldsymbol{M}^{-1}(\boldsymbol{Z}-\boldsymbol{J}\boldsymbol{Q})(\boldsymbol{Z}-\boldsymbol{J}\boldsymbol{Q})^{\mathrm{H}}\right]/\gamma\right\}}{\pi^{NK}\gamma^{NK}|\boldsymbol{M}|^K}. \tag{3}$$

And the PDF under hypothesis H_1 can also be expressed as

$$f_0(\boldsymbol{Z}) = \frac{\exp\left\{-\mathrm{tr}\left[\boldsymbol{M}^{-1}(\boldsymbol{Z}-\boldsymbol{B}\boldsymbol{D})(\boldsymbol{Z}-\boldsymbol{B}\boldsymbol{D})^{\mathrm{H}}\right]/\gamma\right\}}{\pi^{NK}\gamma^{NK}|\boldsymbol{M}|^K} \tag{4}$$

where $\boldsymbol{D}=[\boldsymbol{P}^{\mathrm{T}}\ \boldsymbol{Q}^{\mathrm{T}}]^{\mathrm{T}}$ with $\boldsymbol{P} = [\boldsymbol{p}_1, \boldsymbol{p}_2, \cdots, \boldsymbol{p}_K]$ and $\boldsymbol{Q} = [\boldsymbol{q}_1, \boldsymbol{q}_2, \cdots, \boldsymbol{q}_K]$; $|\cdot|$ and $\mathrm{tr}(\cdot)$ imply the determinant and trace of a square matrix, respectively. Moreover, let $\boldsymbol{\Theta} = [\boldsymbol{\Theta}_{\mathrm{r}}^{\mathrm{T}}, \boldsymbol{\Theta}_{\mathrm{s}}^{\mathrm{T}}]^{\mathrm{T}} \in \mathbf{C}^{(pK+qK+1)\times 1}$ with $\boldsymbol{\Theta}_{\mathrm{r}} = \mathrm{vec}(\boldsymbol{P}) \in \mathbf{C}^{pK\times 1}$ and $\boldsymbol{\Theta}_{\mathrm{s}} = [\gamma, \mathrm{vec}^{\mathrm{T}}(\boldsymbol{Q})]^{\mathrm{T}} \in \mathbf{C}^{(qK+1)\times 1}$, where $\mathrm{vec}(\cdot)$ represents the vectorization of a matrix.

Then the Gradient test for complex-valued signals [31] is given by

$$\lambda_1 = \left.\frac{\partial \ln f_1(\boldsymbol{Z})}{\partial \boldsymbol{\Theta}_{\mathrm{r}}^{\mathrm{T}}}\right|_{\boldsymbol{\Theta}=\hat{\boldsymbol{\Theta}}_0} (\hat{\boldsymbol{\Theta}}_{\mathrm{r}1} - \boldsymbol{\Theta}_{\mathrm{r}0}) \underset{\mathrm{H}_0}{\overset{\mathrm{H}_1}{\gtrless}} T_1 \tag{5}$$

where λ_1 and T_1 denote the detection statistic and threshold, respectively; $\hat{\boldsymbol{\Theta}}_0$ is the ML estimate of $\boldsymbol{\Theta}$ under hypothesis H_0; $\boldsymbol{\Theta}_{\mathrm{r}0}$ is the value of $\boldsymbol{\Theta}_{\mathrm{r}}$ under hypothesis H_0, $\hat{\boldsymbol{\Theta}}_{\mathrm{r}1}$ is the ML estimation of $\boldsymbol{\Theta}_{\mathrm{r}}$ under hypothesis H_1. We can directly obtain $\boldsymbol{\Theta}_{\mathrm{r}0} = \boldsymbol{0}$ because the target is absent under hypothesis H_0.

Taking the derivative of the logarithm of (4) with respect to $\boldsymbol{\Theta}_{\mathrm{r}}$ results in

$$\left.\frac{\partial \ln f_1(\boldsymbol{Z})}{\partial \boldsymbol{\Theta}_{\mathrm{r}}^{\mathrm{T}}}\right|_{\boldsymbol{\Theta}=\hat{\boldsymbol{\Theta}}_0} = \frac{1}{\gamma}[\mathrm{vec}(((\boldsymbol{Z} - \boldsymbol{J}\hat{\boldsymbol{Q}}_0)^{\mathrm{H}}\boldsymbol{M}^{-1}\boldsymbol{H})^{\mathrm{T}})]^{\mathrm{T}}. \tag{6}$$

Performing the derivative of (3) with respect to $\boldsymbol{Q}$, and then setting the result to be zero, it yields the ML estimate of $\boldsymbol{Q}$ under hypothesis H_0:

$$\hat{\boldsymbol{Q}}_0 = (\bar{\boldsymbol{J}}^{\mathrm{H}}\bar{\boldsymbol{J}})^{-1}\bar{\boldsymbol{J}}^{\mathrm{H}}\bar{\boldsymbol{Z}} \tag{7}$$

where $\bar{\boldsymbol{J}} = \boldsymbol{M}^{-1/2}\boldsymbol{J}$, $\bar{\boldsymbol{Z}} = \boldsymbol{M}^{-1/2}\boldsymbol{Z}$. Then (6) can be rewritten as

$$\left.\frac{\partial \ln f_1(\boldsymbol{Z})}{\partial \boldsymbol{\Theta}_{r}^{\mathrm{T}}}\right|_{\boldsymbol{\Theta}=\hat{\boldsymbol{\Theta}}_0} = \frac{1}{\gamma}[\mathrm{vec}((\bar{\boldsymbol{Z}}^{\mathrm{H}}\boldsymbol{P}_{\bar{\boldsymbol{J}}}^{\perp}\bar{\boldsymbol{H}})^{\mathrm{T}})]^{\mathrm{T}} \tag{8}$$

where $\boldsymbol{P}_{\bar{\boldsymbol{J}}}^{\perp} = \boldsymbol{I}_N - \bar{\boldsymbol{J}}(\bar{\boldsymbol{J}}^{\mathrm{H}}\bar{\boldsymbol{J}})^{-1}\bar{\boldsymbol{J}}^{\mathrm{H}}$ with $\boldsymbol{I}_m$ implying an $m \times m$ identity matrix, $\bar{\boldsymbol{H}} = \boldsymbol{M}^{-1/2}\boldsymbol{H}$.

To obtain the detection statistic, it is necessary to acquire $\hat{\boldsymbol{\Theta}}_{\mathrm{r}1}$ in (5). According to (4), the ML estimate of $\boldsymbol{D}$ under hypothesis H_1 can be obtained [21] as follows:

$$\hat{\boldsymbol{D}}_1 = (\bar{\boldsymbol{B}}^{\mathrm{H}}\bar{\boldsymbol{B}})^{-1}\bar{\boldsymbol{B}}^{\mathrm{H}}\bar{\boldsymbol{Z}} \tag{9}$$

where $\bar{\boldsymbol{B}} = \boldsymbol{M}^{-1/2}\boldsymbol{B}$. Note that the ML estimate of $\boldsymbol{P}$ under hypothesis H_1, denoted by $\hat{\boldsymbol{P}}_1$, is the first p columns of $\hat{\boldsymbol{D}}_1$. In the sequel, we try to obtain $\hat{\boldsymbol{P}}_1$ from (9). It is straightforward to confirm

$$\bar{\boldsymbol{B}}^{\mathrm{H}}\bar{\boldsymbol{B}} = \begin{bmatrix} \bar{\boldsymbol{H}}^{\mathrm{H}}\bar{\boldsymbol{H}} & \bar{\boldsymbol{H}}^{\mathrm{H}}\bar{\boldsymbol{J}} \\ \bar{\boldsymbol{J}}^{\mathrm{H}}\bar{\boldsymbol{H}} & \bar{\boldsymbol{J}}^{\mathrm{H}}\bar{\boldsymbol{J}} \end{bmatrix}. \tag{10}$$

For convenience, the inverse of $\bar{\boldsymbol{B}}^{\mathrm{H}}\bar{\boldsymbol{B}}$ is denoted by

$$\boldsymbol{C} = \begin{bmatrix} \boldsymbol{C}_{11} & \boldsymbol{C}_{12} \\ \boldsymbol{C}_{21} & \boldsymbol{C}_{22} \end{bmatrix} \tag{11}$$

where $\boldsymbol{C}_{11} = [\bar{\boldsymbol{H}}^{\mathrm{H}}\bar{\boldsymbol{H}} - \bar{\boldsymbol{H}}^{\mathrm{H}}\bar{\boldsymbol{J}}(\bar{\boldsymbol{J}}^{\mathrm{H}}\bar{\boldsymbol{J}})^{-1}\bar{\boldsymbol{J}}^{\mathrm{H}}\bar{\boldsymbol{H}}]^{-1}$ and $\boldsymbol{C}_{12} = -\boldsymbol{C}_{11}\bar{\boldsymbol{H}}^{\mathrm{H}}\bar{\boldsymbol{J}}(\bar{\boldsymbol{J}}^{\mathrm{H}}\bar{\boldsymbol{J}})^{-1}$, which can be obtained by the matrix inversion lemma [22]. Hence, we have

$$\hat{\boldsymbol{P}}_1 = \boldsymbol{C}_{11}\bar{\boldsymbol{H}}^{\mathrm{H}}\bar{\boldsymbol{Z}} + \boldsymbol{C}_{12}\bar{\boldsymbol{J}}^{\mathrm{H}}\bar{\boldsymbol{Z}} = \left(\bar{\boldsymbol{H}}^{\mathrm{H}}\boldsymbol{P}_{\bar{\boldsymbol{J}}}^{\perp}\bar{\boldsymbol{H}}\right)^{-1}\bar{\boldsymbol{H}}^{\mathrm{H}}\boldsymbol{P}_{\bar{\boldsymbol{J}}}^{\perp}\bar{\boldsymbol{Z}}. \tag{12}$$

Accordingly, we have

$$\hat{\boldsymbol{\Theta}}_{r1} = \mathrm{vec}(\hat{\boldsymbol{P}}_1) = \mathrm{vec}((\bar{\boldsymbol{H}}^{\mathrm{H}}\boldsymbol{P}_{\bar{\boldsymbol{J}}}^{\perp}\bar{\boldsymbol{H}})^{-1}\bar{\boldsymbol{H}}^{\mathrm{H}}\boldsymbol{P}_{\bar{\boldsymbol{J}}}^{\perp}\bar{\boldsymbol{Z}}). \tag{13}$$

Note that $\boldsymbol{\Theta}_{\mathrm{r}0} = \boldsymbol{0}$. Substituting (8) and (13) into (5), after some algebra and simplification, we obtain Gradient test for given γ as

$$\lambda_1 = \frac{1}{\gamma}\mathrm{tr}\left(\bar{\boldsymbol{Z}}^{\mathrm{H}}\boldsymbol{P}_{\boldsymbol{P}_{\bar{\boldsymbol{J}}}^{\perp}\bar{\boldsymbol{H}}}\bar{\boldsymbol{Z}}\right) \underset{\mathrm{H}_0}{\overset{\mathrm{H}_1}{\gtrless}} T_1 \tag{14}$$

where $\boldsymbol{P}_{\boldsymbol{P}_{\bar{\boldsymbol{J}}}^{\perp}\bar{\boldsymbol{H}}} = \boldsymbol{P}_{\bar{\boldsymbol{J}}}^{\perp}\bar{\boldsymbol{H}}(\bar{\boldsymbol{H}}^{\mathrm{H}}\boldsymbol{P}_{\bar{\boldsymbol{J}}}^{\perp}\bar{\boldsymbol{H}})^{\mathrm{H}}\bar{\boldsymbol{H}}^{\mathrm{H}}\boldsymbol{P}_{\bar{\boldsymbol{J}}}^{\perp}$.

In the second step, replacing the true covariance matrix $\boldsymbol{M}$ with its ML estimate based on the training data only, i.e.,

$$\boldsymbol{S} = \boldsymbol{Y}\boldsymbol{Y}^{\mathrm{H}} \tag{15}$$

into (14), we can obtain the 2S-Gradient for given γ as

$$\lambda_{\mathrm{2S-Gradient}} = \frac{1}{\gamma}\mathrm{tr}\left(\tilde{\boldsymbol{Z}}^{\mathrm{H}}\boldsymbol{P}_{\boldsymbol{P}_{\tilde{\boldsymbol{J}}}^{\perp}\tilde{\boldsymbol{H}}}\tilde{\boldsymbol{Z}}\right) \underset{\mathrm{H}_0}{\overset{\mathrm{H}_1}{\gtrless}} T_{\mathrm{2S-Gradient}} \tag{16}$$

where $\boldsymbol{P}_{\boldsymbol{P}_{\tilde{\boldsymbol{J}}}^{\perp}\tilde{\boldsymbol{H}}} = \boldsymbol{P}_{\tilde{\boldsymbol{J}}}^{\perp}\tilde{\boldsymbol{H}}(\tilde{\boldsymbol{H}}^{\mathrm{H}}\boldsymbol{P}_{\tilde{\boldsymbol{J}}}^{\perp}\tilde{\boldsymbol{H}})^{\mathrm{H}}\tilde{\boldsymbol{H}}^{\mathrm{H}}\boldsymbol{P}_{\tilde{\boldsymbol{J}}}^{\perp}$ with $\boldsymbol{P}_{\tilde{\boldsymbol{J}}}^{\perp} = \boldsymbol{I}_N - \tilde{\boldsymbol{J}}(\tilde{\boldsymbol{J}}^{\mathrm{H}}\tilde{\boldsymbol{J}})^{-1}\tilde{\boldsymbol{J}}^{\mathrm{H}}$ and $\tilde{\boldsymbol{J}} = \boldsymbol{S}^{-1/2}\boldsymbol{J}$; $\tilde{\boldsymbol{Z}} = \boldsymbol{S}^{-1/2}\boldsymbol{Z}$, $\tilde{\boldsymbol{H}} = \boldsymbol{S}^{-1/2}\boldsymbol{H}$; $\lambda_{\mathrm{2S-Gradient}}$ and $T_{\mathrm{2S-Gradient}}$ denote the detection statistic and threshold after substitution, respectively.

Furthermore, we can obtain two-step Gradient test in HE by letting $\gamma = 1$ in (16) as follows:

$$\lambda_{\mathrm{2S-Gradient-HE}} = \mathrm{tr}\left(\tilde{\boldsymbol{Z}}^{\mathrm{H}}\boldsymbol{P}_{\boldsymbol{P}_{\tilde{\boldsymbol{J}}}^{\perp}\tilde{\boldsymbol{H}}}\tilde{\boldsymbol{Z}}\right) \underset{\mathrm{H}_0}{\overset{\mathrm{H}_1}{\gtrless}} T_{\mathrm{2S-Gradient-HE}} \tag{17}$$

where $\lambda_{\mathrm{2S-Gradient-HE}}$ and $T_{\mathrm{2S-Gradient-HE}}$ denote the detection statistic and detection after substitution in HE, respectively. Note that the detection statistic of 2S-Gradient-HE is just consistent with the 2S-GLRT-HE in [20].

In the following, our focus is to seek the ML estimate of γ under hypothesis H_0, i.e., $\hat{\gamma}_0$, to obtain the final test statistic in PHE. The ML estimate $\hat{\gamma}_0$ is the unique positive solution of the following equation [13]:

$$\sum_{k=1}^{s}\frac{\lambda_{k,0}}{\lambda_{k,0}+\varsigma} = \frac{NK}{K+R} \tag{18}$$

where ς denotes the unknown, s=min(N,K), and $\lambda_{k,0}$ is the kth non-zero eigenvalue of $\tilde{\boldsymbol{Z}}^{\mathrm{H}}\boldsymbol{P}_{\tilde{\boldsymbol{J}}}^{\perp}\tilde{\boldsymbol{Z}}$.

According to (18), substituting $\hat{\gamma}_0$ for γ into (16) results in the two-step Gradient test in PHE:

$$\lambda_{\mathrm{2S-Gradient-PHE}} = \frac{1}{\hat{\gamma}_0}\mathrm{tr}\left(\tilde{\boldsymbol{Z}}^{\mathrm{H}}\boldsymbol{P}_{\boldsymbol{P}_{\tilde{\boldsymbol{J}}}^{\perp}\tilde{\boldsymbol{H}}}\tilde{\boldsymbol{Z}}\right) \underset{\mathrm{H}_0}{\overset{\mathrm{H}_1}{\gtrless}} T_{\mathrm{2S-Gradient-PHE}} \tag{19}$$

where $\lambda_{\mathrm{2S-Gradient-PHE}}$ and $T_{\mathrm{2S-Gradient-PHE}}$ denote the detection statistic and threshold after substitution in PHE, respectively. It is worth mentioning that, both of the proposed detectors possess the CFAR properties under the design assumptions, which will be proved in the next section.

4. CFAR behaviors

In this section, a deep discussion is given on the dependence of the proposed detectors on clutter parameters under the design assumptions. To prove the CFAR properties of the 2S-Gradient-HE and 2S-Gradient-PHE, we first rewrite the quantities $\tilde{\boldsymbol{Z}}^{\mathrm{H}}\boldsymbol{P}_{\boldsymbol{P}_{\tilde{\boldsymbol{J}}}^{\perp}\tilde{\boldsymbol{H}}}\tilde{\boldsymbol{Z}}$ in (16) as

$$\boldsymbol{Z}_\gamma = \tilde{\boldsymbol{Z}}^{\mathrm{H}}\boldsymbol{P}_{\boldsymbol{P}_{\bar{\boldsymbol{J}}}^{\perp}\tilde{\boldsymbol{H}}}\tilde{\boldsymbol{Z}} = \boldsymbol{Z}^{\mathrm{H}}\boldsymbol{F}\boldsymbol{H}(\boldsymbol{H}^{\mathrm{H}}\boldsymbol{F}\boldsymbol{H})^{-1}\boldsymbol{H}^{\mathrm{H}}\boldsymbol{F}\boldsymbol{Z} \tag{20}$$

where $\boldsymbol{F} = \boldsymbol{S}^{-1} - \boldsymbol{S}^{-1}\boldsymbol{J}(\boldsymbol{J}^{\mathrm{H}}\boldsymbol{S}^{-1}\boldsymbol{J})^{-1}\boldsymbol{J}^{\mathrm{H}}\boldsymbol{S}^{-1} \in \mathbf{C}^{N\times N}$. Define $\boldsymbol{J}_{\parallel} = \bar{\boldsymbol{J}}\left(\bar{\boldsymbol{J}}^{\mathrm{H}}\bar{\boldsymbol{J}}\right)^{-1/2} \in \mathbf{C}^{N\times q}$, and then we have $\boldsymbol{J}_{\parallel}^{\mathrm{H}}\boldsymbol{J}_{\parallel} = \boldsymbol{I}_q$. There exists an orthogonal matrix $\boldsymbol{U} = [\boldsymbol{J}_{\parallel}, \boldsymbol{J}_{\perp}] \in \mathbf{C}^{N\times N}$ with $\boldsymbol{J}_{\perp}^{\mathrm{H}}\boldsymbol{J}_{\perp} = \boldsymbol{I}_{N-q}$ and $\boldsymbol{J}_{\perp}^{\mathrm{H}}\boldsymbol{J}_{\parallel} = \boldsymbol{0}_{(N-q)\times q}$; where $\boldsymbol{0}_{m\times n}$ denotes an $m\times n$ zero matrix, and the semi-unitary matrix $\boldsymbol{J}_{\perp} \in \mathbf{C}^{N\times(N-q)}$ can be obtained by the singular value decomposition (SVD) of $\bar{\boldsymbol{J}}$. Let

$$\begin{cases} \widehat{\boldsymbol{Z}} = \boldsymbol{U}^{\mathrm{H}}\boldsymbol{M}^{-1/2}\boldsymbol{Z}_0 \in \mathbf{C}^{N\times K} \\ \widehat{\boldsymbol{H}} = \boldsymbol{U}^{\mathrm{H}}\boldsymbol{M}^{-1/2}\boldsymbol{H} \in \mathbf{C}^{N\times p} \\ \widehat{\boldsymbol{J}} = \boldsymbol{U}^{\mathrm{H}}\boldsymbol{M}^{-1/2}\boldsymbol{J} \in \mathbf{C}^{N\times q} \\ \widehat{\boldsymbol{F}} = \boldsymbol{U}^{\mathrm{H}}\boldsymbol{M}^{1/2}\boldsymbol{F}\boldsymbol{M}^{1/2}\boldsymbol{U} \in \mathbf{C}^{N\times N} \\ \widehat{\boldsymbol{S}} = \boldsymbol{U}^{\mathrm{H}}\boldsymbol{M}^{-1/2}\boldsymbol{S}\boldsymbol{M}^{-1/2}\boldsymbol{U} \in \mathbf{C}^{N\times N} \end{cases} \tag{21}$$

where $\boldsymbol{Z}_0 = \boldsymbol{Z}/\sqrt{\gamma}$. Then, (20) can be recast as

$$\boldsymbol{Z}_\gamma = \gamma\widehat{\boldsymbol{Z}}^{\mathrm{H}}\widehat{\boldsymbol{F}}\widehat{\boldsymbol{H}}(\widehat{\boldsymbol{H}}^{\mathrm{H}}\widehat{\boldsymbol{F}}\widehat{\boldsymbol{H}})^{-1}\widehat{\boldsymbol{H}}^{\mathrm{H}}\widehat{\boldsymbol{F}}\widehat{\boldsymbol{Z}}. \tag{22}$$

Under hypothesis H_0, one can verify that, after whitening, each column of $\widehat{\boldsymbol{Z}}$ is distributed as a zero-mean complex circular Gaussian random vector, with covariance matrix $\boldsymbol{I}_N$, i.e., $\widehat{\boldsymbol{Z}} \sim \mathrm{CN}(\boldsymbol{0}_{N\times R}, \boldsymbol{I}_N)$. Meanwhile, from (15) and (21), after whitening, $\widehat{\boldsymbol{S}}$ obeys a complex central Wishart distribution with R degrees of freedom and scale matrix $\boldsymbol{I}_N$, i.e., $\widehat{\boldsymbol{S}} \sim \mathrm{CW}(R, \boldsymbol{I}_N)$.

Herein, according to (22), let

$$\boldsymbol{Z}'_\gamma = \frac{1}{\gamma}\boldsymbol{Z}_\gamma = \widehat{\boldsymbol{Z}}^{\mathrm{H}}\widehat{\boldsymbol{F}}\widehat{\boldsymbol{H}}(\widehat{\boldsymbol{H}}^{\mathrm{H}}\widehat{\boldsymbol{F}}\widehat{\boldsymbol{H}})^{-1}\widehat{\boldsymbol{H}}^{\mathrm{H}}\widehat{\boldsymbol{F}}\widehat{\boldsymbol{Z}}. \tag{23}$$

Next, we define the inverse of $\widehat{\boldsymbol{S}}$ by

$$\widehat{\boldsymbol{S}}^{-1} = \begin{bmatrix} \boldsymbol{W}_{11} & \boldsymbol{W}_{12} \\ \boldsymbol{W}_{21} & \boldsymbol{W}_{22} \end{bmatrix} \tag{24}$$

where $\boldsymbol{W}_{11} \in \mathbf{C}^{q\times q}$, $\boldsymbol{W}_{12} \in \mathbf{C}^{q\times(N-q)}$, $\boldsymbol{W}_{21} \in \mathbf{C}^{(N-q)\times q}$ and $\boldsymbol{W}_{22} \in \mathbf{C}^{(N-q)\times(N-q)}$ are the submatrix of $\widehat{\boldsymbol{S}}^{-1}$ defined for convenience of the following representation. From (21) and (24), we can rewrite $\widehat{\boldsymbol{F}}$ as

$$\begin{aligned} \widehat{\boldsymbol{F}} &= \boldsymbol{U}^{\mathrm{H}}\boldsymbol{M}^{1/2}[\boldsymbol{S}^{-1} - \boldsymbol{S}^{-1}\boldsymbol{J}(\boldsymbol{J}^{\mathrm{H}}\boldsymbol{S}^{-1}\boldsymbol{J})^{-1}\boldsymbol{J}^{\mathrm{H}}\boldsymbol{S}^{-1}]\boldsymbol{M}^{1/2}\boldsymbol{U} = \\ &\quad \widehat{\boldsymbol{S}}^{-1} - \widehat{\boldsymbol{S}}^{-1}\widehat{\boldsymbol{J}}(\widehat{\boldsymbol{J}}^{\mathrm{H}}\widehat{\boldsymbol{S}}^{-1}\widehat{\boldsymbol{J}})^{-1}\widehat{\boldsymbol{J}}^{\mathrm{H}}\widehat{\boldsymbol{S}}^{-1} = \\ &\quad \widehat{\boldsymbol{S}}^{-1} - \widehat{\boldsymbol{S}}^{-1}\boldsymbol{E}_1(\boldsymbol{E}_1^{\mathrm{H}}\widehat{\boldsymbol{S}}^{-1}\boldsymbol{E}_1)^{-1}\boldsymbol{E}_1^{\mathrm{H}}\widehat{\boldsymbol{S}}^{-1} = \\ &\quad \begin{bmatrix} \boldsymbol{0}_{q\times q} & \boldsymbol{0}_{q\times(N-q)} \\ \boldsymbol{0}_{(N-q)\times q} & \widehat{\boldsymbol{S}}_{22}^{-1} \end{bmatrix} \end{aligned} \tag{25}$$

with $\boldsymbol{E}_1 = [\boldsymbol{I}_q, \boldsymbol{0}_{q\times(N-q)}]^{\mathrm{T}}$ and $\widehat{\boldsymbol{S}}_{22} = (\boldsymbol{W}_{22} - \boldsymbol{W}_{21}\boldsymbol{W}_{11}^{-1}\boldsymbol{W}_{12})^{-1}$, which is just the submatrix composed of last $N-q$ rows and last $N-q$ columns of $\widehat{\boldsymbol{S}}$, by the matrix inversion lemma [22]. We also use $\widehat{\boldsymbol{J}} = \boldsymbol{E}_1(\boldsymbol{J}^{\mathrm{H}}\boldsymbol{M}^{-1}\boldsymbol{J})^{1/2}$ in the derivation of (25). Substituting the above result into (23), we can obtain

$$\boldsymbol{Z}'_\gamma = \widehat{\boldsymbol{Z}}_2^{\mathrm{H}}\widehat{\boldsymbol{S}}_{22}^{-1}\widehat{\boldsymbol{H}}_2\left(\widehat{\boldsymbol{H}}_2^{\mathrm{H}}\widehat{\boldsymbol{S}}_{22}^{-1}\widehat{\boldsymbol{H}}_2\right)^{-1}\widehat{\boldsymbol{H}}_2^{\mathrm{H}}\widehat{\boldsymbol{S}}_{22}^{-1}\widehat{\boldsymbol{Z}}_2 \tag{26}$$

where $\widehat{\boldsymbol{H}}_2$ and $\widehat{\boldsymbol{Z}}_2$ are the last $N-q$ rows of $\widehat{\boldsymbol{H}}$ and $\widehat{\boldsymbol{Z}}$, respectively. It is straightforward to verify that, under hypothesis H_0, due to the orthogonal matrix $\boldsymbol{U}$ and the whitening matrix $\boldsymbol{M}^{-1/2}$, $\widehat{\boldsymbol{Z}}_2$ and $\widehat{\boldsymbol{M}}_{22}$ are distributed as $\widehat{\boldsymbol{Z}}_2 \sim \mathrm{CN}(\boldsymbol{0}_{(N-q)\times R}, \boldsymbol{I}_{N-q})$ and $\widehat{\boldsymbol{S}}_{22} \sim \mathrm{CW}(R, \boldsymbol{I}_{N-q})$, respectively.

In what follows, using the matrix $\widehat{\boldsymbol{H}}_2$, we can construct a unitary matrix in the form as $\boldsymbol{V} = \left[\widehat{\boldsymbol{H}}_{2_\parallel}, \widehat{\boldsymbol{H}}_{2_\perp}\right] \in \mathbf{C}^{(N-q)\times(N-q)}$ with $\widehat{\boldsymbol{H}}_{2_\parallel}^{\mathrm{H}}\widehat{\boldsymbol{H}}_{2_\parallel} = \boldsymbol{I}_p$ and $\widehat{\boldsymbol{H}}_{2_\perp}^{\mathrm{H}}\widehat{\boldsymbol{H}}_{2_\parallel} = \boldsymbol{0}_{(N-p-q)\times p}$; where $\widehat{\boldsymbol{H}}_{2_\parallel} = \widehat{\boldsymbol{H}}_2\left(\widehat{\boldsymbol{H}}_2^{\mathrm{H}}\widehat{\boldsymbol{H}}_2\right)^{-1/2} \in \mathbf{C}^{(N-q)\times p}$, and $\widehat{\boldsymbol{H}}_{2_\perp} \in \mathbf{C}^{(N-q)\times(N-p-q)}$ is a semi-unitary matrix, which can be obtained by SVD of $\widehat{\boldsymbol{H}}_2$. Denote $\widehat{\boldsymbol{Z}}_{2_V} = \boldsymbol{V}^{\mathrm{H}}\widehat{\boldsymbol{Z}}_2$, $\widehat{\boldsymbol{M}}_{22_V} = \boldsymbol{V}^{\mathrm{H}}\widehat{\boldsymbol{M}}_{22}\boldsymbol{V}$, $\boldsymbol{E}_2 = \left[\boldsymbol{I}_p^{\mathrm{T}}, \boldsymbol{0}_{(N-p-q)\times p}^{\mathrm{T}}\right]^{\mathrm{T}}$. Then (26) can be rewritten as

$$\boldsymbol{Z}'_\gamma = \widehat{\boldsymbol{Z}}_{2_V}^{\mathrm{H}}\widehat{\boldsymbol{M}}_{22_V}^{-1}\boldsymbol{E}_2(\boldsymbol{E}_2^{\mathrm{H}}\widehat{\boldsymbol{M}}_{22_V}^{-1}\boldsymbol{E}_2)^{-1}\boldsymbol{E}_2^{\mathrm{H}}\widehat{\boldsymbol{M}}_{22_V}^{-1}\widehat{\boldsymbol{Z}}_{2_V} \tag{27}$$

with $\boldsymbol{V}^{\mathrm{H}}\widehat{\boldsymbol{H}}_2 = \boldsymbol{E}_2(\widehat{\boldsymbol{H}}_2^{\mathrm{H}}\widehat{\boldsymbol{H}}_2)^{1/2}$ used. Under hypothesis H_0, thanks to the unitary transformation of $\boldsymbol{V}$, $\widehat{\boldsymbol{Z}}_{2_V}$ and $\widehat{\boldsymbol{M}}_{22_V}$ are distributed as

$$\begin{cases} \widehat{\boldsymbol{Z}}_{2_V} \sim \mathrm{CN}(\boldsymbol{0}_{(N-q)\times R}, \boldsymbol{I}_{N-q}) \\ \widehat{\boldsymbol{M}}_{22_V} \sim \mathrm{CW}(R, \boldsymbol{I}_{N-q}) \end{cases}. \tag{28}$$

Combining (27) and (28), we therefore conclude that the statistical property of $\boldsymbol{Z}'_\gamma$ does not depend on $\boldsymbol{M}$ and γ under hypothesis H_0. Then, it is straightforward to conclude that the 2S-Gradient-HE is CFAR against $\boldsymbol{M}$, for $\gamma = 1$, according to (17), (20), and (23).

Next, suppose $\lambda_{k,1}$ is the kth non-zero eigenvalue of $\tilde{\boldsymbol{Z}}^{\mathrm{H}}\boldsymbol{P}_{\bar{\boldsymbol{J}}}^{\perp}\tilde{\boldsymbol{Z}}/\gamma$. By comparing $\tilde{\boldsymbol{Z}}^{\mathrm{H}}\boldsymbol{P}_{\bar{\boldsymbol{J}}}^{\perp}\tilde{\boldsymbol{Z}}$ with $\tilde{\boldsymbol{Z}}^{\mathrm{H}}\boldsymbol{P}_{\bar{\boldsymbol{J}}}^{\perp}\tilde{\boldsymbol{Z}}/\gamma$, it is easy to find that $\lambda_{k,0} = \gamma\lambda_{k,1}$. Therefore, if $\hat{\varsigma}_0$ is the solution of the following equation:

$$\sum_{k=1}^{s}\frac{\lambda_{k,1}}{\lambda_{k,1}+\varsigma} = \frac{NK}{K+R}, \tag{29}$$

then $\gamma\hat{\varsigma}_0$ will also be the solution of (18), i.e., $\hat{\gamma}_0 = \gamma\hat{\varsigma}_0$.

Note that $\hat{\varsigma}_0$ depends neither on $\boldsymbol{M}$ nor on γ under hypothesis H_0, thanks to the independence of $\tilde{\boldsymbol{Z}}^{\mathrm{H}}\boldsymbol{P}_{\bar{\boldsymbol{J}}}^{\perp}\tilde{\boldsymbol{Z}}/\gamma$ on $\boldsymbol{M}$ and γ, which can be proved in the following manner:

$$\tilde{\boldsymbol{Z}}^{\mathrm{H}}\boldsymbol{P}_{\tilde{\boldsymbol{J}}}^{\perp}\tilde{\boldsymbol{Z}}/\gamma=\boldsymbol{Z}^{\mathrm{H}}\boldsymbol{F}\boldsymbol{Z}/\gamma=\hat{\boldsymbol{Z}}^{\mathrm{H}}\boldsymbol{F}\hat{\boldsymbol{Z}}=\hat{\boldsymbol{Z}}_2^{\mathrm{H}}\hat{\boldsymbol{M}}_{22}^{-1}\hat{\boldsymbol{Z}}_2=\hat{\boldsymbol{Z}}_{2_V}^{\mathrm{H}}\hat{\boldsymbol{M}}_{22_V}^{-1}\hat{\boldsymbol{Z}}_{2_V}. \tag{30}$$

Then, substituting $\hat{\gamma}_0=\gamma\hat{\varsigma}_0$ into (18) results in

$$\lambda_{\mathrm{2S-Gradient-PHE}}=\frac{1}{\hat{\varsigma}_0}\mathrm{tr}\left(\boldsymbol{Z}_{\gamma}'\right)\underset{\mathrm{H_0}}{\overset{\mathrm{H_1}}{\gtrless}}T_{\mathrm{2S-Gradient-PHE}}. \tag{31}$$

Hence, the 2S-Gradient-PHE possesses the CFAR property with respect to unknown clutter covariance matrix $\boldsymbol{M}$ and the scaling factor γ.

5. Numerical results

In this section, several numerical results are conducted by Monte Carlo simulations, to investigate the performance of the proposed 2S-Gradient-HE and 2S-Gradient-PHE. To alleviate computation complexity, we set $P_{\mathrm{fa}}=10^{-3}$. $\boldsymbol{P}$ and $\boldsymbol{Q}$ are randomly generated as non-zero matrices. The (i,j)th element of clutter covariance matrix is set as $[\boldsymbol{M}]_{i,j}=\rho^{|i-j|}(i,j=1,2,\cdots,N)$, where ρ is the clutter one-lag correlation coefficient. The signal to clutter ratio (SCR) and the interference to clutter ratio (ICR) are respectively defined as

$$\mathrm{SCR}=\frac{1}{K\gamma}\mathrm{tr}(\boldsymbol{P}^{\mathrm{H}}\boldsymbol{H}^{\mathrm{H}}\boldsymbol{M}^{-1}\boldsymbol{H}\boldsymbol{P}) \tag{32}$$

and

$$\mathrm{ICR}=\frac{1}{K\gamma}\mathrm{tr}(\boldsymbol{Q}^{\mathrm{H}}\boldsymbol{J}^{\mathrm{H}}\boldsymbol{M}^{-1}\boldsymbol{J}\boldsymbol{Q}). \tag{33}$$

Set $\gamma=2$ in PHE, if not specified. In addition, four typical models of multiple dominant scatterers (MDS) are discussed, as shown in Table 1 [32], where only h_0 out of K range cells have target signals components.

Table 1 Target energy distribution of h_0 range cells for different MDS models

Model number	Range cell number			
	1	2	⋯	h_0
Model 1	$1/h_0$	$1/h_0$	⋯	$1/h_0$
Model 2	0.5	$0.5/(h_0-1)$	⋯	$0.5/(h_0-1)$
Model 3	0.9	$0.1/(h_0-1)$	⋯	$0.1/(h_0-1)$
Model 4	1	0	⋯	0

For simplification, in subsequence, the abbreviation 2S-Gradient is indiscriminately used to indicate the proposed detector in HE or PHE, unless otherwise stated.

5.1 CFAR assessment

In order to verify the CFAR properties of the 2S-Gradient, the curves of probability of false alarm P_{fa} versus detection threshold for different clutter parameters involving ρ and γ is shown in Fig. 1. Obviously, all curves with different parameters overlap each other. This means that the proposed detectors both possess the CFAR properties under the design assumptions, which is consistent with the theoretical analyses in Section 4.

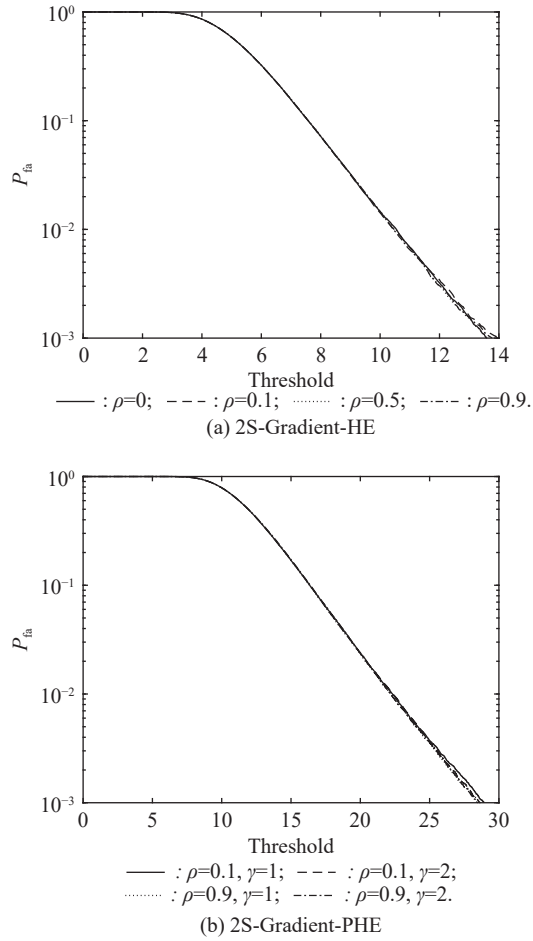

Fig. 1 P_{fa} versus threshold of S-Gradient in HE or PHE for N=8, K=15, R=16, p=3, q=2, ρ=0,0.1,0.5,0.9, h_0=3, ICR=15 dB, γ=1,2

5.2 Influence of target parameters

In Fig. 2, we assess the effect of four typical MDS models on the 2S-Gradient (i.e., probability of detection P_{d} versus SCR curve). It is obvious that the 2S-Gradient tests perform the same for different MDS models in Table 1, which implies that the proposed detectors can avoid the "collapsing loss" [33] usually resulting from an unresolved point-like target, in both HE and PHE. Moreover, Fig. 3 depicts the curves of P_{d} versus SCR for h_0=3,7,10,12. It is shown that the 2S-Gradient tests have almost the same detection performance for different values of h_0, which also indicates the robustness of proposed detectors to different MDS models.

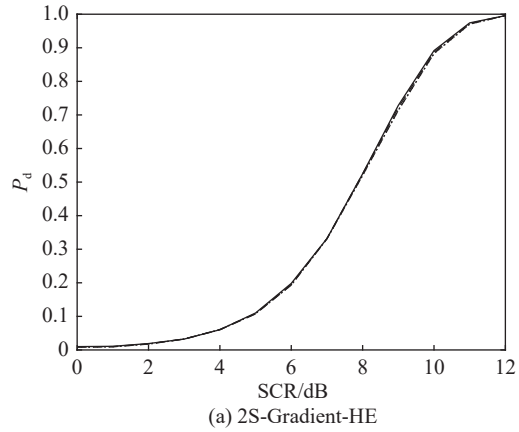

(a) 2S-Gradient-HE

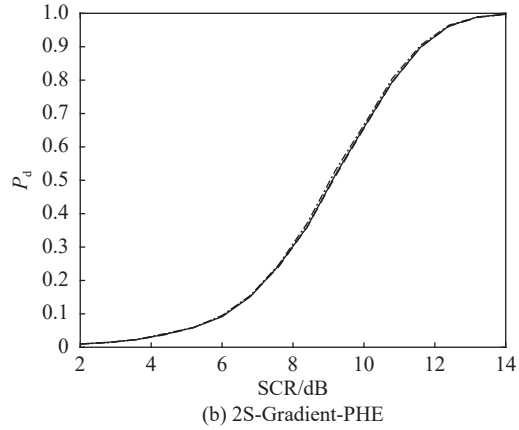

(b) 2S-Gradient-PHE

—— : Model 1; – – – : Model 2; ····· : Model 3; –·–·– : Model 4.

Fig. 2 P_d versus SCR of 2S-Gradient tests in HE and PHE with Model 1−Model 4 for N=8, K=15, R=16, p=3, q=2, P_{fa}=10^{-3}, ρ=0.9, h_0=3, γ=2, ICR=15 dB

In addition, the detection performance of 2S-Gradient is shown for various orders of target subspace (p=2, 3,4,5). Refer to Fig. 4, it can be seen that the performance is degraded with increasing p for both Gradient-based detectors, which may be explained as that increasing p leads to an increase in the number of estimated parameters of unknown $\boldsymbol{P}$.

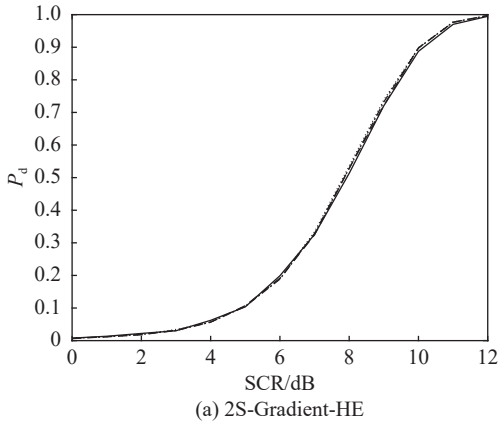

(a) 2S-Gradient-HE

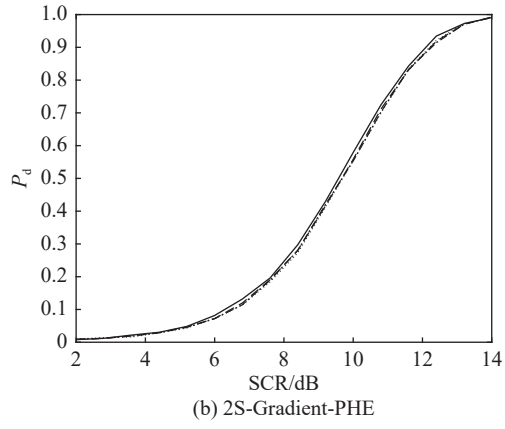

(b) 2S-Gradient-PHE

—— : h_0=3; – – – : h_0=7; ····· : h_0=10; –·–·– : h_0=12.

Fig. 3 P_d versus SCR of 2S-Gradient tests in HE and PHE for N=8, K=15, R=16, p=3, q=2, P_{fa}=10^{-3}, h_0=3,7,10,12, ρ=0.9, γ=2, ICR=15 dB

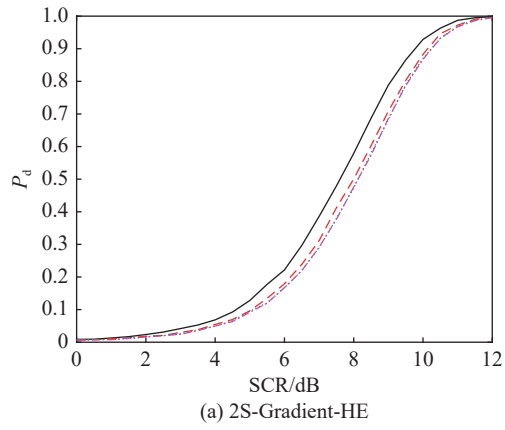

(a) 2S-Gradient-HE

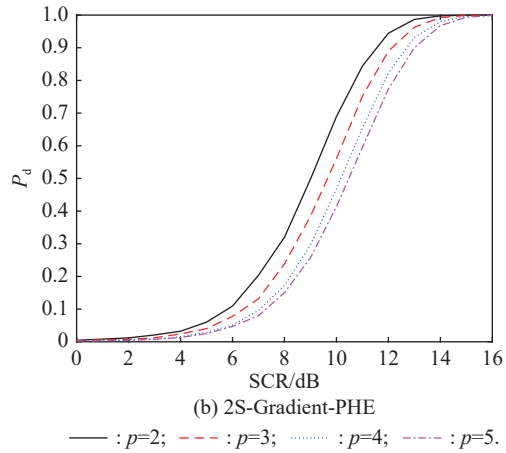

(b) 2S-Gradient-PHE

—— : p=2; – – – : p=3; ····· : p=4; –·–·– : p=5.

Fig. 4 P_d versus SCR of 2S-Gradient tests in HE and PHE for N=8, K=15, R=16, p=2,3,4,5, q=2, P_{fa}=10^{-3}, h_0=3, ρ=0.9, γ=2, ICR=15 dB

5.3 Influence of interference and clutter parameters

Fig. 5 depicts the curves of P_d against SCR with ICR= 5 dB, 10 dB, 15 dB, 20 dB. It highlights that the 2S-Gradient tests can effectively reject interference due to the

results that four curves coincide with each other for different ICRs in both HE and PHE. Fig. 6 analyses detection performance for different clutter one-lag correlation coefficients. The numerical results imply that the proposed detectors are robust to variations of the clutter correlation.

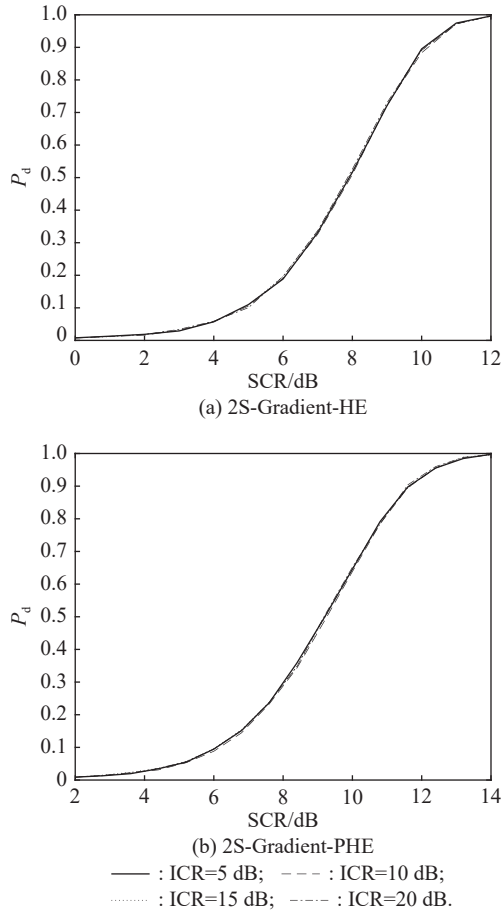

Fig. 5 P_d versus SCR of 2S-Gradient tests in HE and PHE for N=8, K=15, R=16, p=3, q=2, P_{fa}=10^{-3}, h_0=3, ρ=0.9, γ=2, ICR=5, 10 ,15, 20 dB

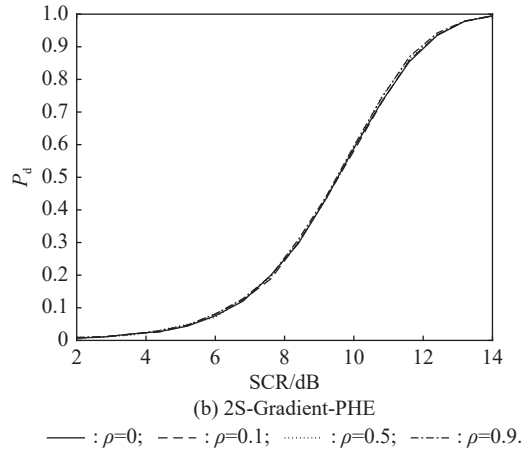

Fig. 6 P_d versus SCR of 2S-Gradient tests in HE and PHE for N=8, K=15, R=16, p=3, q=2, P_{fa}=10^{-3}, h_0=3, ρ=0, 0.1, 0.5, 0.9, γ=2, ICR=15 dB

Fig. 7 explores the influence of N and R on the detection performance of the 2S-Gradient. On the one hand, when R is constant, the detection probability decreases with the increase of N. One possible explanation is that an increase in N means an increase in the dimension of the estimated $\boldsymbol{M}$, which further leads to the decline in estimation accuracy of unknown $\boldsymbol{M}$. On the other hand, the results shows that the detection performance improves as R increases in either HE or PHE for a fixed N, due to the fact that larger R leads to a more accurate estimate of unknown $\boldsymbol{M}$.

Fig. 8 plots the curves of P_d against SCR with different orders of interference subspace (q=2,3,4,5). Analogous to Fig. 4, the performance degenerates with increasing q, which may come from the fact that increasing q leads to an increasing number of estimated parameters of unknown $\boldsymbol{Q}$.

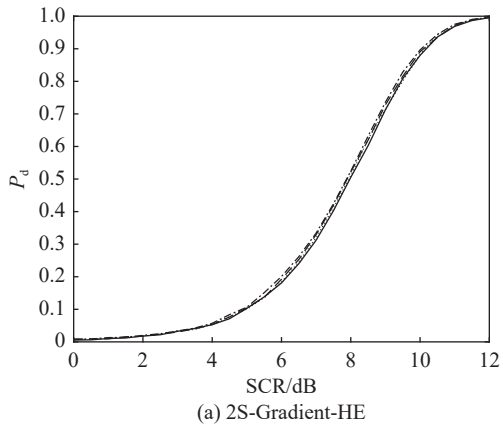

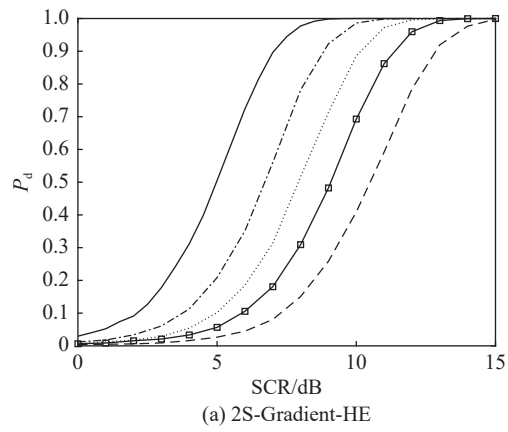

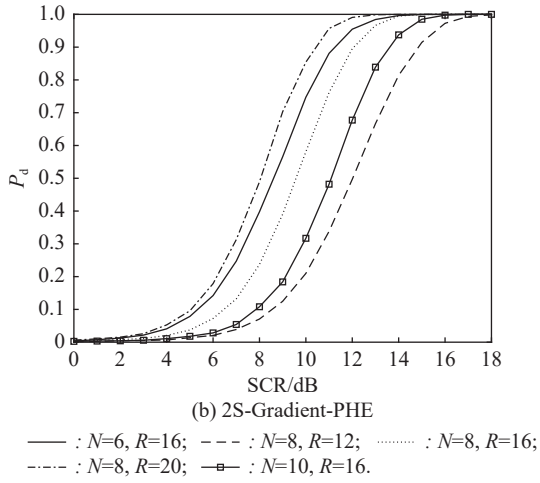

Fig. 7 P_d versus SCR of 2S-Gradient tests in HE and PHE for N=6,8,10, K=15, R=12,16,20, p=3, q=2, $P_{fa}=10^{-3}$, h_0=3, ρ=0.9, γ=2, ICR=15 dB

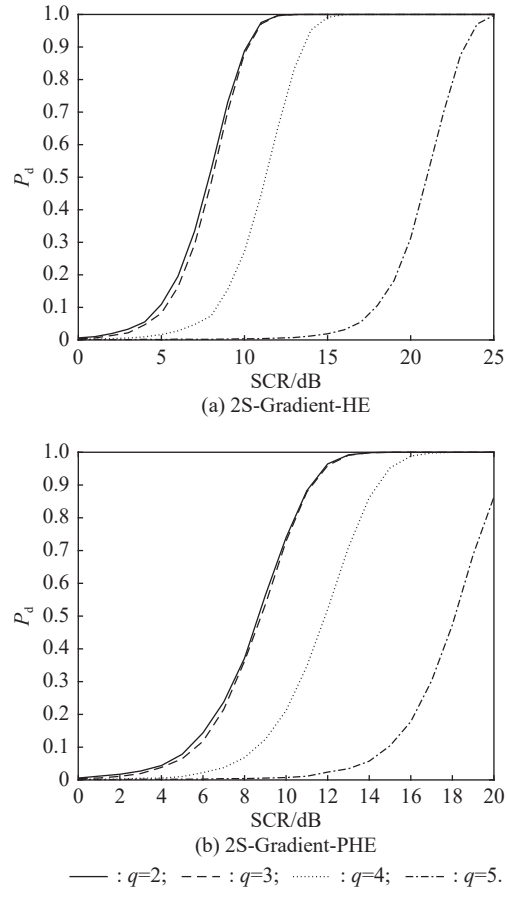

Fig. 8 P_d versus SCR of 2S-Gradient tests in HE and PHE for N=8, K=15, R=16, p=3, q=2,3,4,5, $P_{fa}=10^{-3}$, h_0=3, ρ=0.9, γ=2, ICR=15 dB

5.4 Performance comparison in HE

In this subsection, we assess the proposed 2S-Gradient-HE, by comparison with the existing subspace detectors for the detection problem in HE indicated as (1) and (2), including 1S-GLRT-HE [20], 1S-Rao-HE [21], 2S-Rao-HE [21], 1S-Wald-HE [22], and Gradient-HE [23]. Note that the 1S-Wald-HE are designed for point-like targets and the Gradient-HE has not taken the interference into account.

Additionally, there are a number of potential reasons why the nominal signal subspace matrix $\boldsymbol{H}$ deviates from the actual one $\boldsymbol{H}_A$, including wavefront distortions and array calibration errors [24−26]. Therefore, we also take the mismatched case into account in the following performance comparisons, and use the squared cosine of the mismatch angle ϕ between the actual subspace $\boldsymbol{H}_A$ and the nominal value $\boldsymbol{H}$ in the whitening space to measure the degree of mismatch, i.e.,

$$\cos^2\phi = \frac{\left|\mathrm{tr}\left(\boldsymbol{H}_A\boldsymbol{M}^{-1}\boldsymbol{H}\right)\right|^2}{\mathrm{tr}\left(\boldsymbol{H}_A^{\mathrm{H}}\boldsymbol{M}^{-1}\boldsymbol{H}_A\right)\mathrm{tr}\left(\boldsymbol{H}^{\mathrm{H}}\boldsymbol{M}^{-1}\boldsymbol{H}\right)}. \tag{34}$$

Note that the SCR in the mismatched case is expressed for HE as $\mathrm{SCR}' = \mathrm{tr}(\boldsymbol{P}^{\mathrm{H}}\boldsymbol{H}_A^{\mathrm{H}}\boldsymbol{M}^{-1}\boldsymbol{H}_A\boldsymbol{P})/K$.

Fig. 9 shows P_d of different detectors versus SCR in HE for the matched case. It highlights that under the assumed circumstances, the 2S-Gradient-HE have the similar detection performance with the 2S-Rao-HE and performs better than the other detectors. Fig. 10 shows P_d of different detectors versus SCR′ in HE for a typical mismatched case ($\cos^2\phi$=0.3). It can be seen that the proposed 2S-Gradient-HE performs the best when the mismatch occurs.

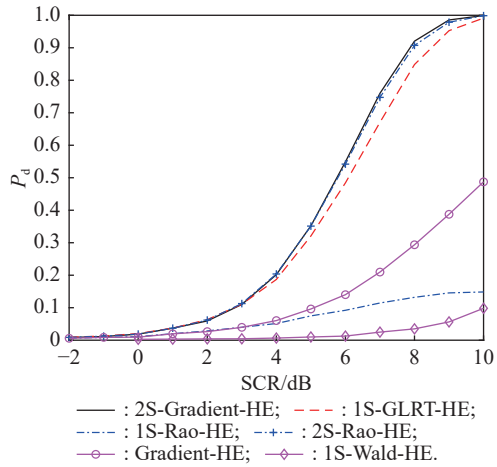

Fig. 9 P_d versus SCR of different detectors in HE for N=8, K=15, R=24, p=3, q=2, $P_{fa}=10^{-3}$, h_0=3, ρ=0.9, ICR=15 dB

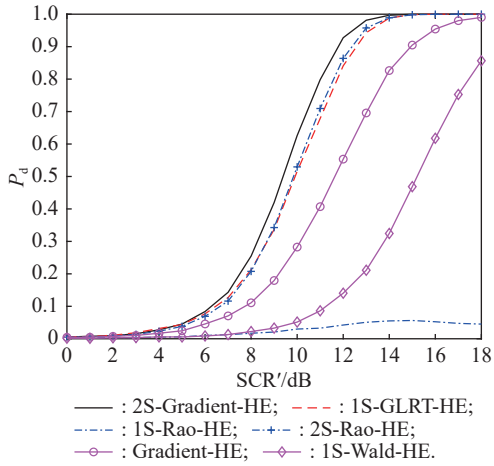

Fig. 10 P_d **versus SCR′ of different detectors in HE for** N**=8,** K**=15,** R**=16,** p**=3,** q**=2,** $P_{fa}=10^{-3}$**,** h_0**=3,** ρ**=0.9, ICR=15 dB,** $\cos^2\phi$**=0.3**

Furthermore, to evaluate mismatch performance, Fig.11 shows P_d versus $\cos^2\phi$ for a given SCR′. It can be seen that the Gradient test proposed in HE possesses strong robustness against the steering vector mismatches, and performs better than the other detectors under different degrees of mismatch. In addition, Fig.12 shows mesa plots of constant detection probability in the mismatched cases. To avoid curves overcrowding in Fig.12, only 2S-Gradient-HE, 1S-GLRT-HE and 2S-Rao-HE are shown, because the three detectors perform better in the previous comparisons. It can be found that, as the mismatch degree increases, all detectors need increasing the values of SCR′ to maintain the same value of P_d. However, the increased values of SCR′ for 2S-Gradient-HE is the least among them, and is almost limited within 2 dB, which also exhibits the best robustness of 2S-Gradient-HE to different mismatched cases.

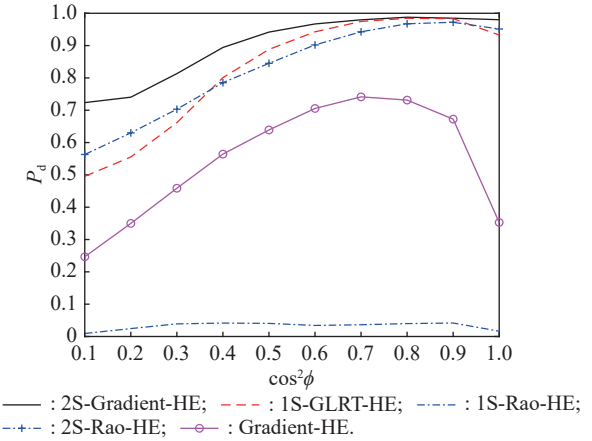

Fig. 11 P_d **versus** $\cos^2\phi$ **of different detectors in HE for** N**=8,** K**=15,** R**=16,** p**=3,** q**=2,** $P_{fa}=10^{-3}$**,** h_0**=3,** ρ**=0.9, ICR=15 dB, SCR′=11 dB**

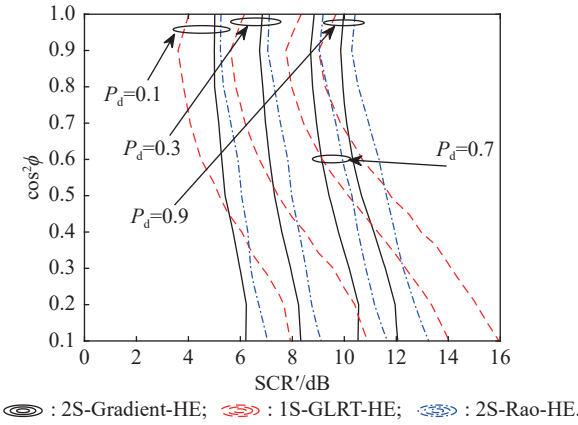

Fig. 12 MESA plots of constant detection probability in HE for N**=8,** K**=15,** R**=16,** p**=3,** q**=2,** $P_{fa}=10^{-3}$**,** h_0**=3,** ρ**=0.9, ICR=15 dB**

5.5 Performance comparison in PHE

Herein, we compare the proposed 2S-Gradient-PHE with the existing detectors designed for PHE including 1S-GLRT-PHE [20], 2S-GLRT-PHE [20], 1S-Rao-PHE [21], 2S-Rao-PHE [21], 1S-Wald-PHE [22], and Gradient-PHE [23]. Note that the 1S-Wald-PHE are derived for point-like targets and the Gradient-PHE does not consider interference. In addition, the signal-to-clutter ratio in the mismatched case is expressed for PHE as $\mathrm{SCR}' = \mathrm{tr}(\boldsymbol{P}^{\mathrm{H}}\boldsymbol{H}_A^{\mathrm{H}}\boldsymbol{M}^{-1}\boldsymbol{H}_A\boldsymbol{P})/(K\gamma)$.

Similarly, Fig. 13 and Fig. 14 show P_d of different PHE detectors versus SCR for matched case and versus SCR′ for mismatched case, respectively. It can be seen that under the assumed circumstances, for either matched or mismatched case, the 2S-Gradient-PHE performs better than the other detectors.

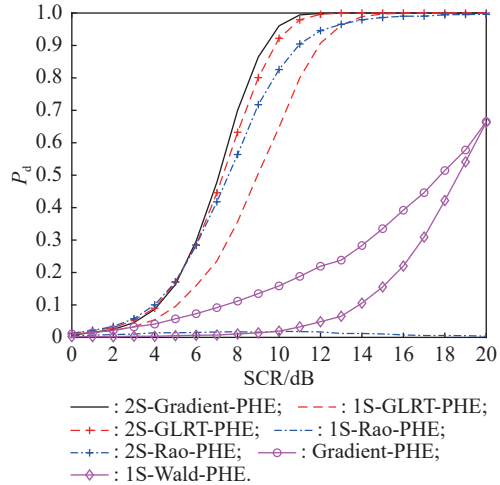

Fig. 13 P_d **versus SCR of different detectors in PHE for** N**=8,** K**=15,** R**=24,** p**=3,** q**=2,** $P_{fa}=10^{-3}$**,** h_0**=3,** ρ**=0.9,** γ**=2, ICR=15 dB**

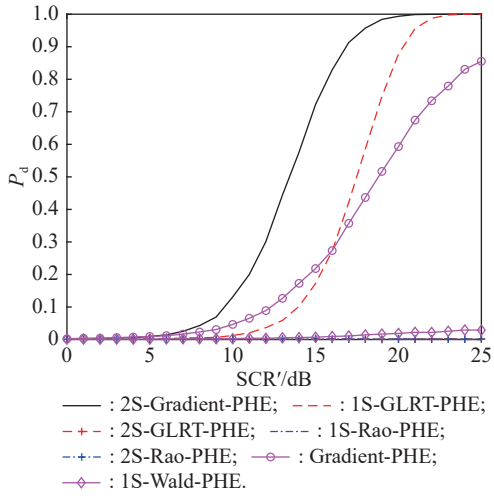

Fig. 14 P_d versus SCR′ of different detectors in PHE for N=8, K=15, R=16, p=3, q=2, $P_{fa}=10^{-3}$, h_0=3, ρ=0.9, γ=2, ICR=15 dB, $\cos^2\phi$=0.3

Fig. 15 further shows P_d versus $\cos^2\phi$ for a given SCR′. It implies that the 2S-Gradient-PHE performs robustly to the steering vector mismatches, and outperforms the other PHE detectors for different mismatched cases. Furthermore, for concise display, Fig.16 only shows mesa plots of constant detection probability in different mismatched cases for representative PHE detectors, including the 2S-Gradient-PHE, 1S-GLRT-PHE, 2S-GLRT-PHE and 2S-Rao-PHE. We can see that all detectors require additional SCR′ to achieve the same detection probability for different mismatch degrees, but the variations of SCR′ for 2S-Gradient-HE is the smallest and always less than 6 dB. These results indicate the strong robustness of 2S-Gradient-PHE to different cases of steering vector mismatch.

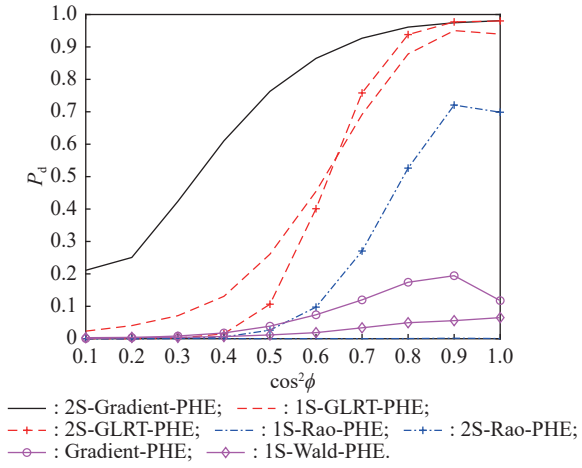

Fig. 15 P_d versus $\cos^2\phi$ of different detectors in PHE for N=8, K=15, R=16, p=3, q=2, $P_{fa}=10^{-3}$, h_0=3, ρ=0.9, γ=2, ICR=15 dB, SCR=13 dB

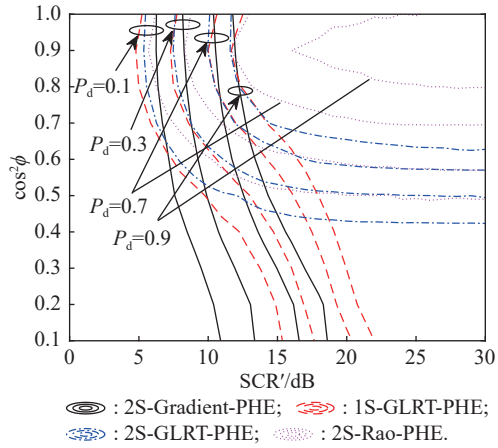

Fig. 16 Mesa plots of constant detection probability in PHE for N=8, K=15, R=16, p=3, q=2, $P_{fa}=10^{-3}$, h_0=3, ρ=0.9, γ=2, ICR=15 dB

6. Conclusions

The problem of adaptively detecting range-spread targets in subspace interference plus Gaussian clutter with unknown covariance matrix is considered for both homogeneous and partially homogeneous environments in this paper. Assume that the target signal and interference signal are modeled as deterministic signals lying in two linearly independent subspaces with unknown coordinates, respectively. According to the two-step Gradient test criteria, for subspace detection of range-spread targets, the 2S-Gradient-HE and 2S-Gradient-PHE are derived in HE and PHE plus structured interference, respectively. Both of the proposed detectors possess CFAR properties respect to unknown clutter covariance matrix as well as the power level. Moreover, two proposed detectors can effectively reject the interference with varying power levels. In addition, the 2S-Gradient tests both performs better than the counterparts under the assumed circumstances, especially in mismatched cases of signal steering vector.

References

[1] JIAN T, HE Y, WANG H P, et al. Persymmetric generalised adaptive matched filter for range-spread targets in homogeneous environment. IET Radar, Sonar & Navigation, 2019, 13(8): 1234–1241.

[2] LIU W J, LIU J, HAO C P, et al. Multichannel adaptive signal detection: basic theory and literature review. Science China Information Sciences, 2022, 65(2): 121301.

[3] HAO C P, ORLANDO D, MA X, et al. Adaptive detection of distributed targets with orthogonal rejection. IET Radar, Sonar & Navigation, 2012, 6(6): 483–493.

[4] JIAN T, HE Y, SU F, et al. Robust detector for range-spread targets in non-Gaussian background. Journal of Systems Engineering and Electronics, 2012, 23(3): 355–363.

[5] XU S W, SHUI P L. Performance analysis of multi-channel order statistics detector for range-spread target. Journal of

Systems Engineering and Electronics, 2012, 23(5): 689–699.
[6] GUO X L, TAO H H, ZHAO H Y, et al. Persymmetric Rao and Wald tests for adaptive detection of distributed targets in compound-Gaussian noise. IET Radar, Sonar & Navigation, 2017, 11(3): 453–458.
[7] LIU W J, XIE W C, LIU J, et al. Adaptive double subspace signal detection in Gaussian background—Part I: homogeneous environments. IEEE Trans. on Signal Processing, 2014, 62(9): 2345–2357.
[8] DE MAIO A, IOMMELLI S. Coincidence of the Rao test, Wald test, and GLRT in partially homogeneous environment. IEEE Signal Processing Letters, 2008, 15: 385–388.
[9] LIU J, JIAN T, LIU W J. Persymmetric detection of subspace signals based on multiple observations in the presence of subspace interference. Signal Processing, 2021, 183: 107964.
[10] ORLANDO D, RICCI G. A Rao test with enhanced selectivity properties in homogeneous scenarios. IEEE Trans. on Signal Processing, 2010, 58(10): 5385–5390.
[11] SHUAI X F, KONG L J, YANG J Y. Adaptive detection for distributed targets in Gaussian noise with Rao and Wald tests. Science China Information Sciences, 2012, 55(6): 1290–1300.
[12] HAO C P, MA X C, SHANG X Q, et al. Adaptive detection of distributed targets in partially homogeneous environment with Rao and Wald tests. Signal Processing, 2012, 92(4): 926–930.
[13] WANG Z Y, LI M, CHEN H M, et al. Persymmetric detectors of distributed targets in partially homogeneous disturbance. Signal Processing, 2016, 128: 382–388.
[14] FOGLIA G, HAO C P, FARINA A, et al. Adaptive detection of point-like targets in partially homogeneous clutter with symmetric spectrum. IEEE Trans. on Aerospace and Electronic Systems, 2017, 53(4): 2110–2119.
[15] GAO Y C, MAO L L, ZHU S Q, et al. Subspace detection for range-spread target to suppress interference: exploiting persymmetry in non-homogeneous scenario. Journal of Systems Engineering and Electronics, 2022, 33(1): 60–71.
[16] GAO Y C, LIAO G S, LIU W J. High-resolution radar detection in interference and nonhomogeneous noise. IEEE Signal Processing Letters, 2016, 23(10): 1359–1363.
[17] MAO L L, GAO Y C, YAN S F, et al. Persymmetric subspace detection in structured interference and non-homogeneous disturbance. IEEE Signal Processing Letters, 2019, 26(6): 928–932.
[18] DONG Y L, LIU M, LI K, et al. Adaptive direction detection in deterministic interference and partially homogeneous noise. IEEE Signal Processing Letters, 2017, 24(5): 599–603.
[19] GAO Y C, LIAO G S, LIU W J, et al. Bayesian generalised likelihood ratio tests for distributed target detection in interference and noise. IET Radar, Sonar & Navigation, 2017, 11(5): 752–758.
[20] BANDIERA F, DE MAIO A, GRECO A S. Adaptive radar detection of distributed targets in homogeneous and partially homogeneous noise plus subspace interference. IEEE Trans. on Signal Processing, 2007, 55(4): 1223–1237.
[21] LIU W J, LIU J, HUANG L. Rao tests for distributed target detection in interference and noise. Signal Processing, 2015, 117: 333–342.
[22] LIU W J, LIU J, LI H, et al. Multichannel signal detection based on Wald test in subspace interference and Gaussian noise. IEEE Trans. on Aerospace and Electronic Systems, 2019, 55(3): 1370–1381.
[23] TANG P Q, DONG R, LIU W J. Adaptive multichannel detectors for distributed target based on gradient test. Signal Processing, 2022, 191: 108350.
[24] LIU J, LI J. Mismatched signal rejection performance of the persymmetric GLRT detector. IEEE Trans. on Signal Processing, 2019, 67(6): 1610–1619.
[25] SUN S Y, LIU J, LIU W J, et al. Robust detection of distributed targets based on Rao test and Wald test. Signal Processing, 2021, 180: 107801.
[26] COLUCCIA A, FASCISTA A, RICCI G. A novel approach to robust radar detection of range-spread targets. Signal Processing, 2020, 166: 107223.
[27] JIAN T, HE J, LIU Y, et al. Persymmetric adaptive detection of range-spread targets in subspace interference plus Gaussian clutter. Science China Information Sciences, 2023, 66(5): 152306.
[28] LIU J, LIU W J, CHEN X, et al. Performance analysis of the generalized likelihood ratio test in general phased array radar configuration. IEEE Trans. on Signal Processing, 2021, 69: 4544–4555.
[29] LIU J, SUN S Y, LIU W J. One-step persymmetric GLRT for subspace signals. IEEE Trans. on Signal Processing, 2019, 67(14): 3639–3648.
[30] LIU J, MASSARO D, ORLANDO D, et al. Radar adaptive detection architectures for heterogeneous environments. IEEE Trans. on Signal Processing, 2020, 68: 4307–4319.
[31] SUN M R, LIU W J, LIU J, et al. Complex parameter Rao, Wald, Gradient, and Durbin tests for multichannel signal detection. IEEE Trans. on Signal Processing, 2022, 70: 117–131.
[32] JIAN T, HE Y, SU F, et al. Adaptive detection of range-spread targets without secondary data in multichannel autoregressive process. Digital Signal Processing, 2013, 23(5): 1686–1694.
[33] CONTE E, DE MAIO A, RICCI G. GLRT-based adaptive detection algorithms for range-spread targets. IEEE Trans. on Signal Processing, 2001, 49(7): 1336–1348.

Biographies

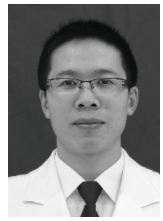

JIAN Tao was born in 1980. He received his B.S., M.S., and Ph.D. degrees in electronic engineering from Naval Aeronautical and Astronautical University (NAAU), Yantai, China, in 2003, 2006, and 2011, respectively. His research interest is radar target adaptive detection.
E-mail: work_jt@163.com

HE Jia was born in 1999. He received his B.S. degree in electronic engineering from the Naval Aviation University, Yantai, China, in 2020, where he is currently pursuing his master's degree. His research interest is radar signal processing.
E-mail: 1191804968@qq.com

WANG Bencai was born in 1980. He received his Ph.D. degree in information and communication engineering, from the Naval Aviation University, Yantai, China in 2011. Since 2013. His research interest is radar signal processing.
E-mail: springbook7559@126.com

LIU Yu was born in 1986. He received his B.S. and Ph.D. degrees in information and communication engineering from the Naval Aviation University, Yantai, China, in 2008 and 2014, respectively. His research interests include radar signal and data processing.
E-mail: liuyu77360132@126.com

XU Congan was born in 1987. He received his M.S. and Ph.D. degrees from Naval Aviation University, Yantai, China, in 2013 and 2016, respectively. His research interests include intelligent perception and fusion, and deep learning and its application.
E-mail: xcatougao@163.com

XIE Zikeng was born in 1998. He received his B.S. degree in systems engineering from the Naval Aviation University, Yantai, China, in 2020, where he is currently pursuing his master's degree. His research interest is radar signal processing
E-mail: 1397850644@qq.com